Assessing Weld Quality in Continuous Ultrasonic Welding of Thermoplastic Composites via In-Situ Monitoring

Johannes M. van Stuyvesant Meijen, Bram C.P. Jongbloed
SAM XL
TU Delft Campus
Rotterdamseweg 382c
2629HG Delft, The Netherlands

ABSTRACT

Continuous ultrasonic welding (CUW) of thermoplastic composites is a novel joining technique able to produce long welded seams at high welding speeds. Our state-of-the-art welding setup entails an industrial robot on a track and an in house developed end effector. Currently no quality inspection methodology has been implemented, therefore it is not known how the weld quality can be correlated to sensor and generator data. Such a method would enable the prediction of the weld quality after the process, and be a steppingstone for closed-loop controlled welding minimizing defects. The goal of the current study is to use two off-the-shelf sensors for in-situ monitoring of the welding process and correlating the sensor data to the weld quality. A laser line scanner is introduced behind the consolidator measuring the step height between the top surfaces of the overlapping adherends. A forward looking infrared (FLIR) camera is introduced looking at the region of the top adherend behind the consolidator. This camera captures the residual heat present in the top adherend. The main findings from this study are that it is possible to use these two sensors to monitor the welding process and that the data acquired from them can be used to make predictions of the weld quality along its length. The thickness of the welded interface, which can be measured from the laser line scanner data, can give an indication of whether the interface is unwelded, welded or overheated. Regarding the FLIR camera, variations in the temperature at the top surface do correspond to variations in the quality of the weld interface, and furthermore, the rate at which the measured temperature changes is positively correlated to the magnitude of the power consumed by the ultrasonic generator. The FLIR camera can therefore be a powerful sensor to determine weld quality and its consistency throughout the length of the weld.

1. INTRODUCTION

The transition towards more sustainable aircraft that are also allowing for reduced costs and higher production rates demands the use of composite materials in aircraft structures. These type of aircraft are highly wanted by airlines given the current societal and environmental needs. Thermoplastic composites are of special interest due to the advantages they have over the more commonly used thermoset composites. The main benefits come in the manufacturing phase, since thermoplastics can repeatedly be molten when heated, and consolidated when cooled. This inherent property of the thermoplastic matrix can introduce significant cost reductions as it opens the doors to efficient forming and joining techniques; take for example the Multifunctional Fuselage Demonstrator (MFFD) within the Clean Sky 2 Programme [1]. Thermoplastic composites can be assembled by creating welded joints as an alternative to mechanical fastening or adhesive bonding. The most

studied welding techniques are resistance, induction and ultrasonic welding, where the latter has been proven to be the most energy and time efficient [2].

In ultrasonic welding, heat is generated through high frequency (between 20 and 50 kHz) and low amplitude (between 10 and 250 µm) mechanical vibrations applied by a metal horn (the sonotrode) onto the weld interface in combination with a static force. Furthermore, to efficiently generate heat at the interface, a layer of the same thermoplastic material as used in the composite parts is placed at the interface. This layer of material, named energy director (ED), will undergo a higher cyclic strain than the fibre reinforced parts, focusing friction heating and viscoelastic heating at the interface [3, 4]. Once the thermoplastic is molten at the interface, the parts are consolidated and cooled under pressure. The ultrasonic welding process can be performed in a continuous way, by translating the sonotrode over the desired length as it applies the mechanical vibrations and the compressive force [5]. This process is known as continuous ultrasonic welding (CUW), and it can make use of a rounded sonotrode for an improved heat concentration at the interface and because it makes circumferential welds possible [6]. The sonotrode is usually followed by a consolidation shoe responsible of cooling the weld and applying sufficient pressure to create a strong bond [7]. A compactor is sometimes placed in front of the sonotrode to dampen the vibrations which travel away from the welding zone and to ensure a better alignment of the parts ahead of the sonotrode.

We developed a robotized setup composed of an industrial robot on a track and an in house developed CUW end effector. This allows the technology to be more fit for industry, as the bench welder used in previous studies [7, 6] was limited to continuous welding along a single axis. In order to guarantee the quality of the welds produced with such a robotic setup, it is necessary to introduce sensors capable of in-situ monitoring the welding process. These sensors should provide meaningful data that can be used to assess the quality of the weld or to indicate the presence of defects right after welding. Such a method for quality inspection is currently lacking in this process, but it's certainly a topic of importance for further development of the technology.

This study is meant as a first step towards in-situ monitoring of the CUW welding process. We introduce a method for direct quality assessment of the weld, using two sensors: a laser line scanner (LLS) and a forward looking infrared (FLIR) camera. Various welds were produced using the robotic CUW setup at SAM XL under varying process parameters to capture differences in the sensor data for varying weld qualities. The quality of the welds was assessed using various test methods, allowing to find a relationship between the data captured during the welding process and the defects found in each weld.

2. RESEARCH TESTS & EXPERIMENTS

2.1. Material

The adherends used for welding were extracted from carbon fibre reinforced polyphenylene sulfide (CF/PPS) thermoplastic composite laminates. The laminates were press consolidated by Toray Advanced Composites (The Netherlands), and are made up of 14 plies of their Toray Cetex® TC1100 UD tape stacked in the following sequence: $[45/0/135/0/0/90/0]_s$. The areal weight of each ply is 145 gsm, with a consolidated ply thickness of 153 µm, leading to a theoretical total thickness of 2.142 mm. The laminates were supplied with dimensions of 1800 mm by 1200 mm, with the 0° fibres running along the longer dimension. Rectangular adherends measuring 500 mm in length and 96.25 mm in width were extracted from these laminates, with the 0° direction along the width. All adherends were cleaned with isopropyl alcohol before welding. The ED used in all welding

experiments was the 766x597/53PW plain woven PPS mesh supplied by PVF GmbH (Germany), with an open area of 53%. The measured thickness was 470 µm, and the measured areal mass was 150 gsm. Once fully flattened, the thickness of this ED would theoretically be 111 µm, computed using the density of PPS (150 gsm ÷ 1.35 g/cm^3 = 111 µm).

2.2. Welding setup and process control

The robotic CUW setup consists of an industrial robotic arm, the KUKA KR560 R3100-2 (from KUKA, Germany), mounted onto a 2 m long linear track developed by Vansichen Linear Technology (Belgium), and a CUW end effector (EEF) developed in house by SAM XL (The Netherlands). Images of the setup are shown in Figure 1.

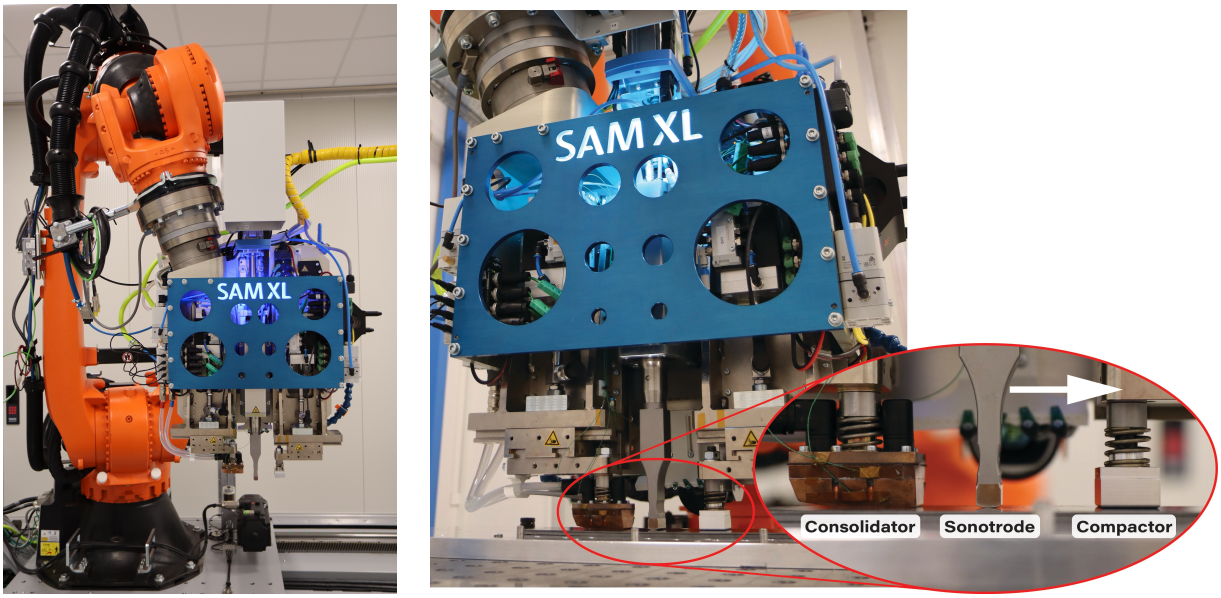

(a) Robotic arm and end effector

(b) End effector and main components for CUW

Figure 1: Robotic setup for CUW at SAM XL

From Figure 1b, one can see the three main components from the EEF used for welding: an actively cooled consolidator, a sonotrode and a compactor. The consolidator is made from copper and actively cooled with water during the welding process. The sonotrode, custom-built by Hermann Ultrasonics (Germany), has a rounded tip along the welding direction with a radius of 17.5 mm, as seen from the side view in Figure 2c. Along its width (normal to the welding direction), the sonotrode features a 30 mm wide surface (Figure 2b), creating only a line of contact between the sonotrode and the top adherend. The mechanical vibrations exerted by the sonotrode are generated by an Ultrabond G7 digital 20/48.20 ultrasonic generator (Hermann Ultrasonics, Germany), operating at 20 kHz. The compactor is made from aluminium, functions as a dampener for vibrations traveling ahead of the sonotrode, and helps align the top adherend.

The adherends are kept in position by means of a so called picture frame jig (Figure 2a), which constrains only the in-plane movement of the adherends. The jig, consisting of an aluminium base, does allow for out-of-plane movement, needed for the downwards displacement of the top adherend during welding as the ED is flattened. Illustrations of this setup can be seen in Figure 2, showing the overlap width of 30 mm, the total width of 162.5 mm, and the weld length of 310 mm used

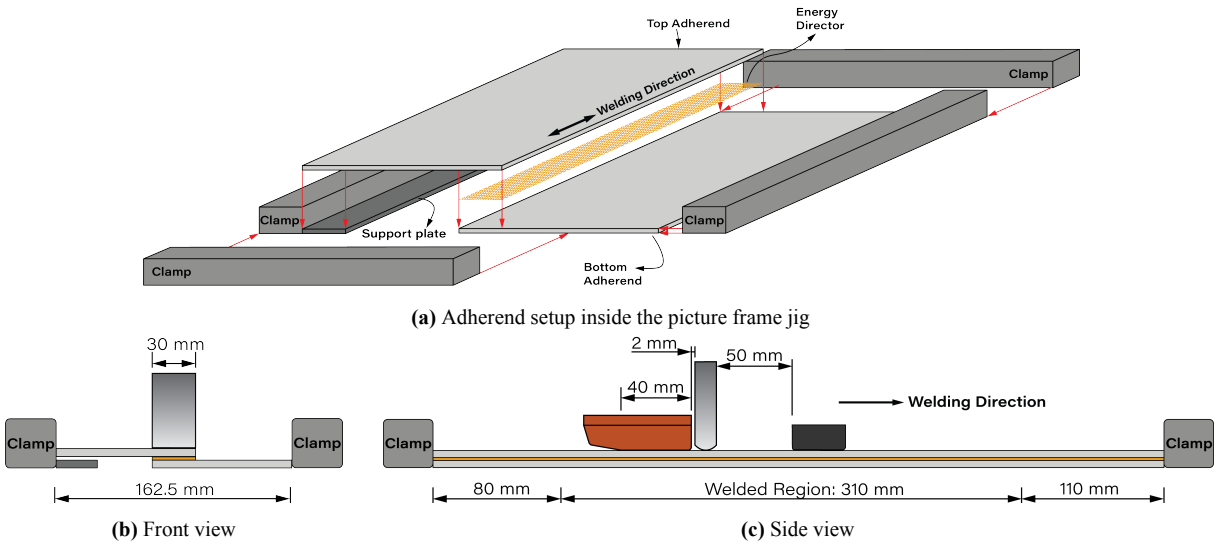

(a) Adherend setup inside the picture frame jig

(b) Front view

(c) Side view

Figure 2: Illustration of the adherend setup inside the picture frame jig used for all the welding experiments

throughout all experiments. Furthermore, a support plate is placed underneath the top adherend, with a thickness equal to that of the bottom adherend.

The consolidator was placed 2 mm behind the sonotrode [6] with a contact surface of 30 mm by 40 mm, and was applying a force of 2160 N, which is equivalent to a consolidation pressure of 1.8 MPa. The compactor was placed 50 mm ahead of the sonotrode, and applied a force of 1000 N on a contact surface of 30 mm by 30 mm. The welding force of the sonotrode was set at 1800 N, and the peak-to-peak amplitude of the vibrations was kept constant at 80 µm. The energy input was controlled by varying the welding speed: higher welding speeds result in less energy consumed by the generator, while lower speeds result in more consumed energy. The welding speeds were varied between 12 mm/s and 20 mm/s, as shown in the text matrix in Table 1.

Table 1: Overview of the welding experiments performed in this study

Welding speed	Amplitude	Remark
12 mm/s	80 µm	Higher heat generation
13 mm/s	80 µm	
14 mm/s	80 µm	
16 mm/s	80 µm	
20 mm/s	80 µm	Lower heat generation

2.3. In-situ monitoring

During each welding process, two sensors were used to capture data in-situ with the goal of finding a new method to make rapid quality assessments of welds. The sensors are: a LLS, of which the laser projection can be seen in Figure 3a; and a FLIR camera, visible in Figure 3b.

The LLS was a scanCONTROL 3010-50 from Micro-Epsilon (Germany), mounted behind the consolidator to record the step profile formed by the two welded adherends behind the consolidator (Figure 3a). Using the software from Micro-Epsilon, it's possible to use this profile to compute the difference in height between the top and the bottom adherend, which would be equivalent to

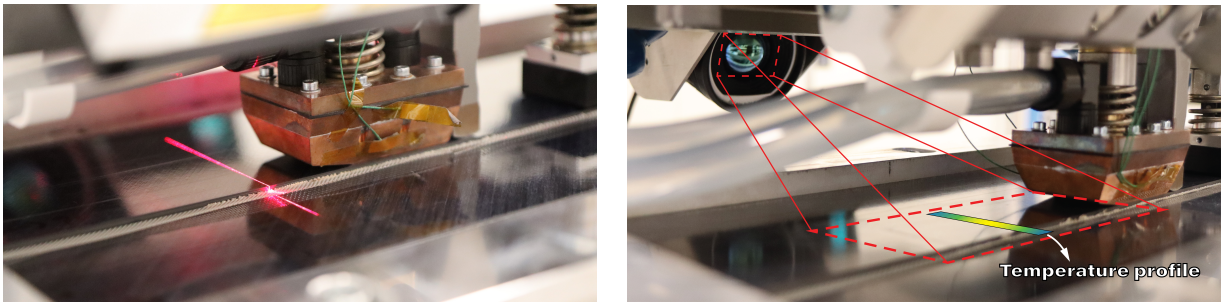

(a) LLS projection to measure step height

(b) FLIR camera focused behind the consolidator

Figure 3: Sensors used in the robotic CUW setup for in-situ monitoring

the thickness of the top adherend plus the interface thickness. This step height was logged at a frequency of 50 Hz for all welds. Prior to welding, the thickness of the top adherend was measured at four points along the interface using a digital micrometer, in order to compute the thickness of the ED or interface once the step height had been measured. Large fluctuations in ED thickness can be a sign of defects and inconsistent quality along the weld.

The FLIR camera was a FLIR A655sc (USA), mounted onto the backplate of the EEF and pointing at the rear side of the consolidator (Figure 3b) to measure the residual temperature at the top surface of the top adherend after welding and consolidating. The camera was recording at 50 fps, and from each single frame, a temperature profile along the width of the weld was measured, using the FLIR basically as temperature line scanner. Since each frame corresponded to a position along the weld length, using all temperature profiles made it possible to recreate the top surface temperature in the form of heat maps. Furthermore, the Pearson correlation coefficient (PCC) was computed between the Power data (P) and the time derivative of the temperature data $\left(\frac{d}{dt}\mathrm{T}\right)$. The temperature data used for this purpose corresponds to the temperature measured over time at the middle point of the overlap width, which was also smoothened by computing a moving average with a window of 10 data points.

2.4. Quality assessment of the welds

After welding, the welded adherends were visually inspected, c-scanned, and cut into coupons for cross-sectional microscopy and for mechanical testing. The c-scans were performed over the full overlaps to visualize porosity at the interface. The welded adherends were then cut along the width into a total of 12 coupons using a water-cooled cutting machine (Compcut ACS 600, England). Ten 25.4 mm wide and 162.5 mm long (equivalent to the total weld width) coupons were used for single-lap-shear (SLS) testing, and two 15 mm wide coupons were used for cross-sectional microscopy. The cross sections (CS) were trimmed to 32 mm long coupons, then embedded in clear epoxy, after which they were prepared using a Tegramin-20 grinding and polishing machine from Struers (Denmark) for posterior inspection with a 3D laser scanning confocal microscope (Keyence VK-X1000, Belgium). The SLS coupons were tested in a 250 kN Zwick/Roell univestal testing machine with a testing speed of 1.14 mm/min. The coupons were placed 25 mm inside each grip, making the grip-to-grip distance equivalent to 112.5 mm. Using the total overlap area (25.4 mm $\times$ 30 mm) and the maximum load of each coupon, the apparent SLS strength was computed. Once tested, images were taken of all fracture surfaces for further quality inspection (fracture mechanism, porosity, unwelded regions, etc) using a Keyence VR 5000 digital microscope (Belgium).

3. RESULTS

3.1. Laser line scanner data for weld quality assessment

The thickness of the welded ED relative to its original thickness is shown in Figure 4 for all the welds. The plot also includes a line marking the theoretical thickness of the ED once fully flattened. Furthermore, examples of matrix and fibre squeeze out at the longitudinal edges of the overlap are also included, where normal ED squeeze out is shown for the 13 mm/s weld and excessive fibre and matrix squeeze out for the 12 mm/s weld. The two cross-sectional microscopy images taken from the 13 mm/s weld are shown in Figure 5. The ED thickness measured by the LLS at these sections can also be identified in the graph from Figure 4, which in both cases was measured to be between 25% and 30% of the original ED thickness. To clearly visualize the interfaces in Figure 5, a close-up detail from each image is also included.

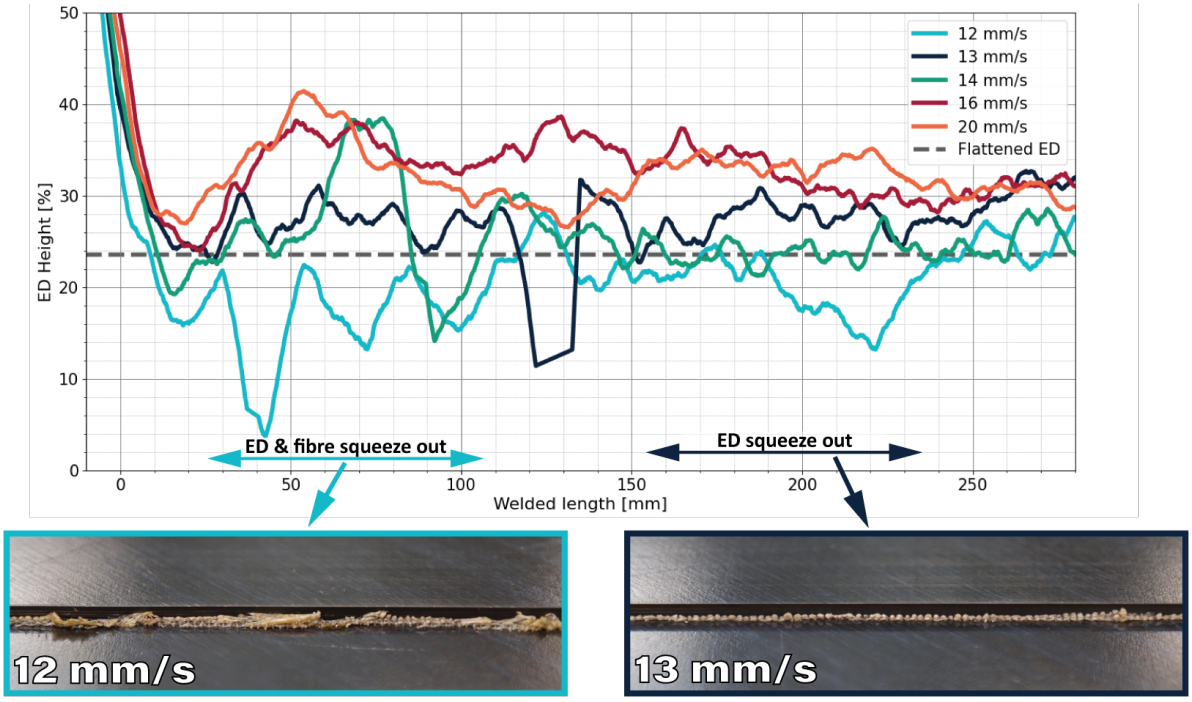

Figure 4: Relative ED thickness measured by the LLS and squeeze out at the weld edge

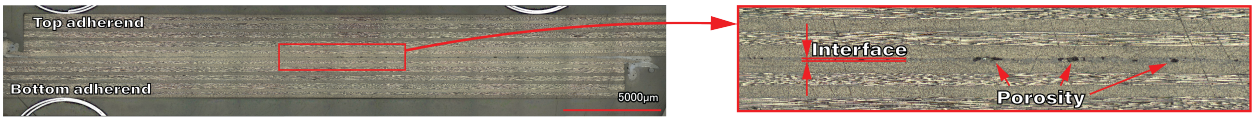

(a) CS at 45 mm from the start of the welded region

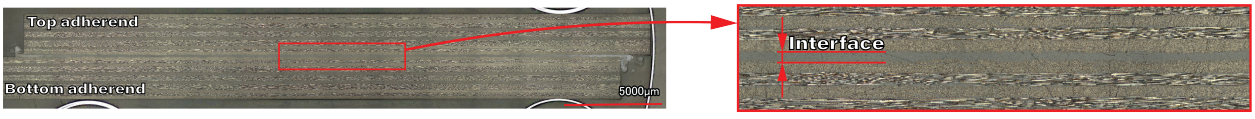

(b) CS at 250 mm from the start of the welded region

Figure 5: Cross sectional microscopy images of the weld performed at 13 mm/s

3.2. FLIR camera data for weld quality assessment

Two of the heat maps created from the videos recorded with the FLIR camera are shown in Figure 6a and Figure 7a for a low speed (13 mm/s) and a high speed (20 mm/s) weld respectively. Figures 6b and 7b show a c-scan from the same welds and Figures 6c and 7c show a corresponding fracture surface extracted from the regions enclosed by a red rectangle.

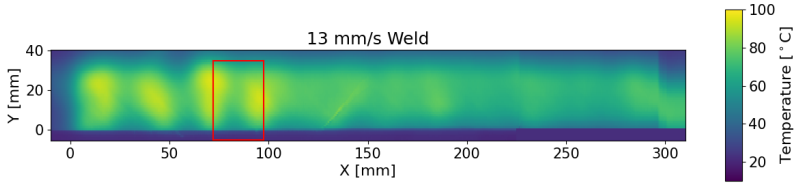

(a) Top surface temperature after consolidation

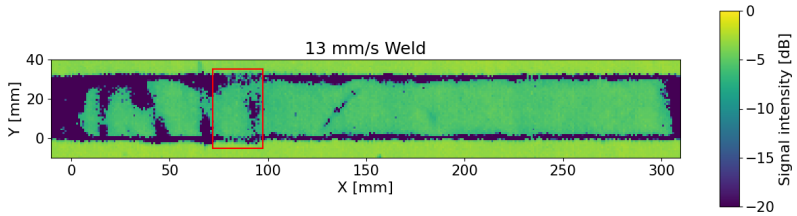

(b) C-scan

(c) Fracture surface

Figure 6: Results from the weld performed at 13 mm/s

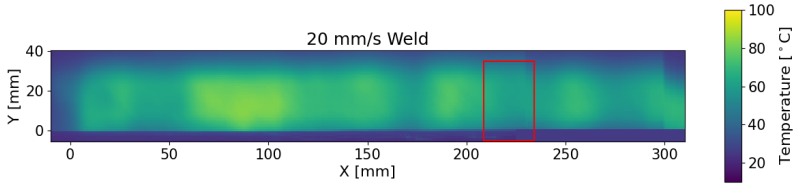

(a) Top surface temperature after consolidation

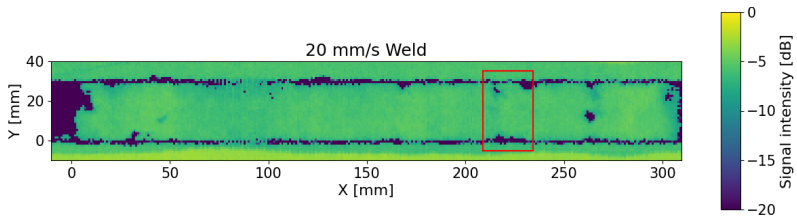

(b) C-scan

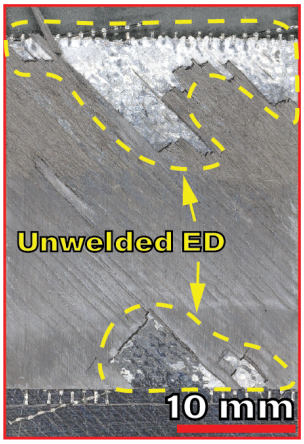

(c) Fracture surface

Figure 7: Results from the weld performed at 20 mm/s

In Figure 8, the top surface temperature at the middle point of the overlap extracted from the FLIR data is plotted together with the power consumed by the ultrasonic generator over the entire length of the welds performed at 13 mm/s and 20 mm/s. The plots show what appears to be a form of correlation between the temperature measured by the FLIR camera and the power taken from the generator data. To further demonstrate the relationship between power and top surface temperature, the PCC was computed between generator power and the time derivative of temperature data. For the 13 mm/s weld (Figure 8a), the PCC was computed to be 0.63, indicating a strong positive correlation; while for the 20 mm/s weld (Figure 8b) the PCC was computed to be 0.38, indicating

a moderate positive correlation. The PCC values for all welds can be found in Table 2, which also includes the average energy density (the integral of the power curve over time divided by the overlap area) and the average SLS strengths.

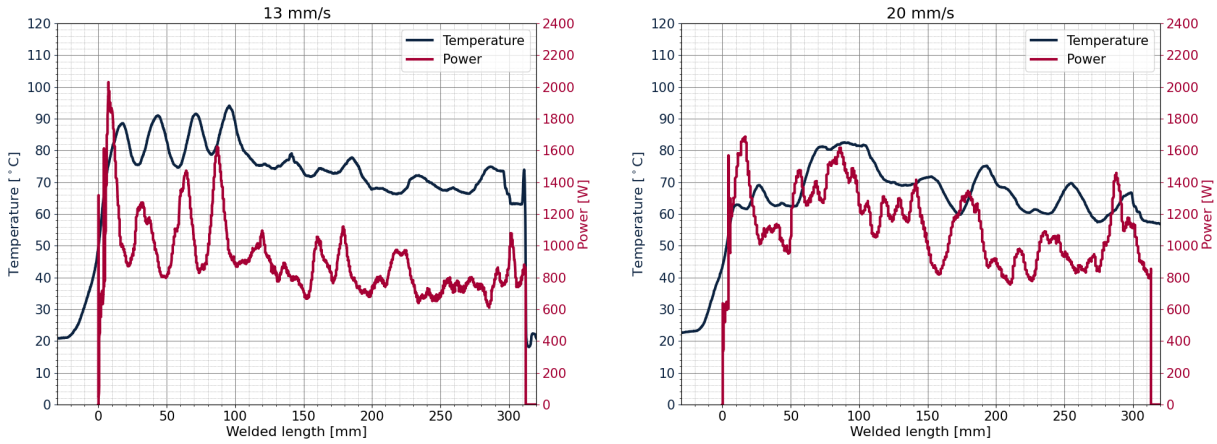

(a) Temperature and power plotted for the 13 mm/s weld

(b) Temperature and power plot for the 20 mm/s weld

Figure 8: Temperature and power plotted over the weld length for a low speed (a) weld and a high speed (b) weld

Table 2: Overview of relevant results

Weld Speed [mm/s]	Energy Density [J/mm^2]	SLS Strength [MPa] (CoV)	PCC $(\mathbf{P}, \frac{\mathbf{d}}{\mathbf{dt}}\mathbf{T})$
12	2.56	28.1 ($\pm$3.5 %)	0.48
13	2.36	29.1 ($\pm$2.1 %)	0.63
14	2.19	30.1 ($\pm$5.0 %)	0.66
16	2.05	29.9 ($\pm$4.4 %)	0.46
20	1.87	28.5 ($\pm$10.7 %)	0.38

4. DISCUSSION

With the aim of testing the use of sensors for in-situ monitoring of the CUW welding process, the results obtained in this study demonstrate that having a LLS and a FLIR camera for this purpose enables a new method to assess the quality of welds in a rapid and non destructive way. The five welds created in this study featured differences in weld quality, which was mainly achieved by the fact that the welds were performed with different welding speeds and hence different amounts of energy for welding (see the energy density for each weld in Table 2). The lower speed welds showed more signs of overheating in the form of fibre squeeze out and voids at the interface, and the higher speed welds showed underwelded regions with unwelded material. Some of these differences were captured by the data provided by the LLS and the FLIR camera.

From the LLS measurements shown in Figure 4, it is possible to see where portions of the weld interface have become thinner than the threshold defined by the theoretical flattened ED thickness

(indicated by the dashed line). It has been observed from the edges of the welds that the weld line thickness only drops below this value in combination with large amounts of fibre and matrix squeeze out at the edges. The squeeze out at the two edges shown in Figure 4 are a good example of this, where the weld performed at 12 mm/s clearly shows larger amounts of ED at the edge when the ED height is low, compared to the edge shown from the 13 mm/s weld where the ED height stays above the threshold. In general, for the lower speed welds, where more energy was consumed by the generator, the weld line thickness can drop below this threshold, indicating that fibres might have been squeezed out and porosity due to material degradation is likely to be present. The reason for the threshold to exist is the fact that the ED alone can not flow out of the interface, because of the large distance (30 mm width) along which the ED would have to flow in order to reach the edges and be squeezed out. On the other hand, the welds performed at higher speeds exhibit ED heights well above the threshold, which is an indication of insufficient flattening and hence under-welding. Take for example the 20 mm/s weld, which shows an overall ED height which does not go below 30% of the original ED thickness in combination with unwelded material at the interface (shown in Figure 7c).

The limitation of the LLS, however, is its inability to detect all the regions where porosity did appear. As shown in Figure 5, the weld exhibits porosity at 45 mm of weld length, even if the ED height measured by the LLS is not well below the threshold. This same weld, at 250 mm of weld length, was measured to have a similar ED height by the LLS, but does show a locally much thicker interface from the cross-sectional microscopy image. This result is explained by the fact that the LLS looks at the overall step height between the bottom and the top adherend, which does not account for local variations along the width of the interface. Hence, how one should make use of the LLS data is by checking whether the ED height deviated significantly from the flattened ED threshold in order to identify regions where the material either degraded or did not melt enough. What the specific upper and lower limits of the welded ED thickness should be in order to define a good quality weld should be studied in more depth in future work.

Regarding the thermal measurements, the data gathered from the FLIR camera also gave new insights into the CUW process. In the first example shown in Figure 6, corresponding to the weld performed at 13 mm/s, a clear non-uniform heat distribution was measured at the top adherend, with temperatures ranging from less than 70°C to more than 90°C. The regions where the highest temperatures were recorded correspond to the regions in the c-scan showing the presence of porosity at the interface (those with a low signal intensity). The fracture surface shown in Figure 6c is used to further demonstrate the presence of porosity at the region characterized by higher temperatures.

A second example is shown in Figure 7, which corresponds to the weld performed at 20 mm/s. In this case, fluctuations in temperature of more than 20°C are observed, but with the presence of unwelded ED at the regions of the interface where the temperature was lower (Figure 7c). These unwelded regions, which can not be captured by the c-scan (see Figure 7b), are named kissing bonds, which occur when there is intimate contact between the ED and the adherend, but without molecular inter-diffusion. The use of a FLIR camera could be essential to determine the presence of such unwelded regions, by simply indicating where the temperature was measured to go below a certain threshold.

For the experiments conducted in this test campaign it was not possible to compare the temperatures measured between different welds in an absolute manner, since each weld was cooled for a different duration due to the different welding speeds and thus different exposure durations to the consolidator. Nevertheless, the non uniformity of the temperature measured along a single

weld explains why there can be large fluctuations in weld quality within the same weld. In the 13 mm/s weld for example (Figure 6b), the beginning of the weld is characterized by large regions with voids while the end shows very few signs of porosity. To ensure more consistent and hence better weld qualities, it seems to be important to gain more control over the temperatures reached at the interface. Since the heat dissipates from the interface to the top surface of the top adherend, it might be assumed that a more constant temperature measured by the FLIR camera should also translate to a more consistent weld quality.

It was seen that for some of the welds there seemed to be a strong correlation between the temperature data and the power data from the ultrasonic generator. This is especially visible in the first half of the plot shown in Figure 8a. It was found that a correlation exists between the rate at which the temperature changes and the magnitude of the power: for the welds performed at 13 and 14 mm/s, the Pearson correlation coefficient (see Table 2) was computed to be 0.63 and 0.66 respectively. This coefficient was lower for the weld performed at the lowest speed (12 mm/s) and for those performed at higher speeds (16 and 20 mm/s). In Figure 8b, one can indeed see that the correlation between the two sets of data is much less when welding at 20 mm/s. A possible reason for the lower correlation found at 16 and 20 mm/s could be that heat is still dissipating away from the interface and did not reach the top surface yet, given the smaller period of time (due to higher speeds) between the moment heat is generated and the moment temperature is measured at the top surface. The lower correlation found at 12 mm/s can be explained by the fact that the top surface was cooled down for longer, due to a longer contact with the consolidator, hence giving a worse representation of the temperature development at the interface.

However, the strong correlation seen in two of the welds does imply that the power consumed by the generator does affect the temperature generation at the interface, despite the fact that the welding force and amplitude are kept constant. These fluctuations can be explained by the fact that the viscosity of ED underneath the sonotrode (which is in turn dependent on its temperature or melt state) can vary significantly, constantly changing the mechanical impedance of the material and hence affecting the power required to vibrate the sonotrode at the set amplitude. Especially when welding wider overlaps, it has been noted that larger fluctuations in power correspond to larger differences in the degree to which the ED was molten. This result does provide the new insight that controlling the power consumed by the generator, i.e. having a constant power, could help to generate heat in a more constant manner and to therefore have a more consistent weld quality. We are currently exploring constant power welding to aim for higher weld quality.

5. CONCLUSION

The goal of this study was to test the use of a laser line scanner and a FLIR camera for in-situ monitoring of the continuous ultrasonic welding process to investigate how the data obtained from these sensors could correlate to the weld quality. The laser line scanner was successfully used to record the thickness of the energy director after consolidation, and the FLIR camera recorded the temperature of the top adherend behind the consolidator. The relationship between the measured energy director height and the quality of the welds was studied, concluding that large fluctuations in the height data related to poorer quality of the welds. When the height is reduced to less than the minimum theoretical thickness of the flattened energy director, overheating and fibre squeeze out can be expected, while the opposite implies that underwelded regions can be present at the interface. The temperature measured at the top adherend was found to correlate to the quality of

the welds. The fluctuations in temperature over the length of the weld corresponded to fluctuations in weld quality seen from c-scans and fracture surfaces, meaning that the FLIR camera can be a useful tool to predict quality. It was also found that the top surface temperature, and hence the quality of the weld, has a correlation with the power consumed by the ultrasonic generator. A positive Pearson correlation coefficient was computed between the rate at which the top surface temperature changes and the magnitude of the power. This finding is a motivation to investigate the possibility of welding with a constant power to control the temperature and hence quality.

6. ACKNOWLEDGMENTS

This study was funded by the ENLIGHTEN project (Enabling Integrated Lightweight Structures in High-Volumes) from the Perspectief Initiative by the NWO (Dutch Research Council).

7. REFERENCES

[1] C. Aviation. *Bringing the Next Generation MultiFunctional Fuselage Demonstrator (MFFD) to life*. 2024. URL: https://www.clean-aviation.eu/clean-sky-2/key-demonstrators/multi-functional-fuselage-demonstrator.

[2] I. F. Villegas, L. Moser, A. Yousefpour, P. Mitschang, and H. E. Bersee. "Process and performance evaluation of ultrasonic, induction and resistance welding of advanced thermoplastic composites". In: *Journal of Thermoplastic Composite Materials* Vol. 26.No. 8 (2013). Publisher: SAGE Publications Ltd STM, pp. 1007–1024. ISSN: 0892-7057. DOI: 10.1177/0892705712456031. URL: https://doi.org/10.1177/0892705712456031.

[3] I. F. Villegas. "Ultrasonic Welding of Thermoplastic Composites". In: *Frontiers in Materials* Vol. 6 (2019). ISSN: 2296-8016. URL: https://www.frontiersin.org/articles/10.3389/fmats.2019.00291.

[4] H. Potente. "Ultrasonic welding — Principles & theory". In: *Materials & Design* Vol. 5.No. 5 (1984), pp. 228–234. ISSN: 0261-3069. DOI: 10.1016/0261-3069(84)90032-3. URL: https://www.sciencedirect.com/science/article/pii/0261306984900323.

[5] F. Senders, M. van Beurden, G. Palardy, and I. Fernandez Villegas. "Zero-flow: A novel approach to continuous ultrasonic welding of CF/PPS thermoplastic composite plates". In: *Advanced Manufacturing: Polymer & Composites Science* Vol. 2.No. 3 (2016), pp. 83–92. ISSN: 2055-0340. DOI: 10.1080/20550340.2016.1253968. URL: http://resolver.tudelft.nl/uuid:f3704652-6e5e-4653-84aa-88f1fbd5dc8d.

[6] B. Jongbloed, J. Teuwen, and I. F. Villegas. "On the use of a rounded sonotrode for the welding of thermoplastic composites". In: *Journal of Advanced Joining Processes* Vol. 7 (2023), p. 100144. ISSN: 2666-3309. DOI: 10.1016/j.jajp.2023.100144. URL: https://www.sciencedirect.com/science/article/pii/S2666330923000067.

[7] B. Jongbloed, R. Vinod, J. Teuwen, R. Benedictus, and I. F. Villegas. "Improving the quality of continuous ultrasonically welded thermoplastic composite joints by adding a consolidator to the welding setup". In: *Composites Part A: Applied Science and Manufacturing* Vol. 155 (2022), p. 106808. ISSN: 1359-835X. DOI: 10.1016/j.compositesa.2022.106808. URL: https://www.sciencedirect.com/science/article/pii/S1359835X22000057.